A reduced muscle model and planar musculoskeletal model fit for the simulation of whole-body movements

Matthew Millard *, Anna Lena Emonds, Monika Harant, Katja Mombaur

Optimization, Robotics and Biomechanics (ORB), Institute of Computer Engineering (ZITI), Berliner Str. 45, 69120 Heidelberg, Heidelberg University, Heidelberg, Germany

ARTICLE INFO

ABSTRACT

Musculoskeletal models are made to reflect the capacities of the human body in general, and often a specific subject in particular. It remains challenging to both model the musculoskeletal system and then fit the modelled muscles to a specific human subject. We present a reduced muscle model, a planar musculoskeletal model, and a fitting method that can be used to find a feasible set of active and passive muscle parameters for a specific subject. At a minimum, the fitting method requires inverse dynamics data of the subject, a scalar estimate of the peak activation reached during the movement, and a plausible initial estimate for the strength and flexibility of that subject. While additional data can be used to result in a more accurate fit, this data is not required for the method solve for a feasible fit. The minimal input requirements of the proposed fitting method make it well suited for subjects who cannot undergo a maximum voluntary contraction trial, or for whom recording electromyographic data is not possible. To evaluate the model and fitting method we adjust the musculoskeletal model so that it can perform an experimentally recorded stoop-lift of a 15 kg box.

© 2019 Published by Elsevier Ltd.

1. Introduction

Musculoskeletal models have been used to analyze and synthesize human motion for the purposes of movement science (Steele et al., 2010; Delp et al., 2007; Arnold et al., 2013; Hiley et al., 2015) and the design of assistive technologies (van den Bogert et al., 2012; Millard et al., 2017). People come in different shapes and sizes, and have varying levels of strength and flexibility. The accuracy of a subject-specific model often depends on capturing specific weaknesses (Sreenivasa et al., 2017; Steele et al., 2010), flexibility (Millard et al., 2017), or strengths (King et al., 2006) of the subject. While there are data and algorithms available to accurately estimate the size, mass and inertia properties of a subject's entire body (De Leva, 1996; Jensen, 1986), it remains challenging to model the musculature of the whole-body and to fit these models to a specific subject.

Many parts of the body are difficult to represent in a mathematical model. Lumped-parameter models treat muscle and tendon as groups of massless cables that attach to, and wrap around, the skeleton (Delp et al., 2007). By representing musculotendons as massless cables it is possible to compute the kinematics of muscle fibers and also the internal forces on the body such as bone-on-bone contact forces (Scholz et al., 2014). A single long muscle can be accurately modelled using a single cable. Muscles which are bulky, or resemble sheets, are more challenging to model and often need to be represented using many cables. This approach has been used to develop anatomically detailed models of the legs (Arnold et al., 2010), shoulder (van der Helm, 1997), and back (Christophy et al., 2012; De Zee et al., 2007). Very few anatomically detailed whole-body models have been developed (van den Bogert et al., 2013; Damsgaard et al., 2006; Nakamura et al., 2005). While this high level of anatomic detail is needed to simulate a surgical intervention, or compute bone-on-bone contact forces, it is not necessary for every investigation.

Once a musculoskeletal model has been made the challenging task of fitting it to a specific subject begins. Many muscle model formulations do not afford fitting due to parameter-space singularities (Yeadon et al., 2006; Anderson et al., 2007), and state-space discontinuities (Yeadon et al., 2006; Anderson et al., 2007; Thelen, 2003) in the first and second derivatives. Unfortunately these formulations are difficult to use with gradient-based optimization methods (Wächter and Biegler, 2006; Gill et al., 2005). Although singularity-free muscle model formulations exist (Millard et al., 2013), identifying the parameters that best fit a specific subject is still difficult.

Accurate subject-specific musculoskeletal models have been constructed, though often with the use of equipment or experi-

* Corresponding author.
  E-mail address: matthew.millard@ziti.uni-heidelberg.de (M. Millard).

mental methodology that is not well suited for all subjects. Dynamometers have been used to directly measure the active-torque-angle, torque-velocity, passive-torque-angle curves of the hip, knee and ankle joints in the sagittal plane across a wide variety of subjects (Anderson et al., 2007); the spatial strength of the shoulder, elbow, and wrist of an expert tennis player (Kentel et al., 2011); and the musculature of the legs and arms of an elite gymnast (Hiley et al., 2015). As it is not always possible to make the extensive dynamometry measurements for each subject, optimization has been used by King et al. (2009) to adapt the active muscle characteristics of one elite athlete to another. While dynamometers can directly measure the characteristics of the modelled muscles, these properties can also be inferred when electromyographic (EMG) data is recorded along with trials in which a maximum voluntary contraction (MVC) is reached. When EMG and MVC data is used in combination with inverse dynamics data it is possible to solve for the properties of the modelled muscles using optimization (Lloyd and Besier, 2003; Sartori et al., 2012) or by posing the fitting problem as an optimal-control problem (Falisse et al., 2017). For many subjects, particularly patients, it is not possible to test them in a dynamometer nor perform MVC trials.

Here we focus on developing a reduced muscle model and planar whole-body musculoskeletal model that can be fit to a specific subject and is well suited for motion synthesis. Section 2 begins with a description of the reduced muscle model which includes a number of fitting parameters so that it can be more easily adapted to a specific subject. By using several data sets from the literature, as described in Section 2.1, we have formed estimates for the active and passive properties of 14 muscle groups consistent with a young adult male subject. Our fitting method, described in Section 2.2, extends the work of King et al. (2009) because both the parallel elasticity of the muscle and its active properties are adjusted during the fitting process. The fitting method, which requires neither EMG data nor MVCs, has been developed to make the minimal adjustment to the initial estimate for the muscle parameters such that the torque demands of the recorded motion are feasible. Section 2.3 describes how the method is evaluated by using it to fit the active and passive properties of a musculoskeletal model so that it is strong enough and flexible enough to emulate a subject lifting a 15 kg box off the floor. In addition, the parameters of the 14 muscle groups can be found in Appendix A along with plots that illustrate the torque-angle and torque-velocity characteristics of each muscle group. A detailed fitting example is provided in Appendix B which demonstrates how the fitting routine can be applied to estimate the leg strength of a young clinical patient who walks with crouch gait. To enable others to reproduce and extend our work we have implemented the muscle models and fitting method as part of the muscle package in RBDL,[1] an open-source software library for modeling and simulating multibody systems.

2. Methods

The human body can be approximated as a rigid-body mechanism governed by the differential-algebraic equations (DAEs)

$$M(\mathbf{q})\ddot{\mathbf{q}} + c(\mathbf{q}, \dot{\mathbf{q}}) = \boldsymbol{\tau} + G(\mathbf{q})^T \underline{\lambda} \qquad (1)$$

$$g(\mathbf{q}) = 0 \qquad (2)$$

where $\mathbf{q}, \dot{\mathbf{q}}$, and $\ddot{\mathbf{q}}$ are the generalized positions, velocities, and accelerations of the model; $M(\mathbf{q})$ is the mass matrix, and $c(\mathbf{q}, \dot{\mathbf{q}})$ is the vector of Coriolis and centripetal forces. Kinematic constraints

described in the vector $g(\mathbf{q})$ can be used to describe contact between the body and hard objects (e.g. between the foot and the ground), while the generalized forces these constraints apply to the body are contained in the term $G(\mathbf{q})^T \underline{\lambda}$ where $G(\mathbf{q})$ is the Jacobian of the constraint equations $g(\mathbf{q})$ with respect to $\mathbf{q}$, and $\underline{\lambda}$ is the vector of Lagrange multipliers which are proportional to the constraint forces. In these equations the forces the muscles generate and apply to the body are contained in $\boldsymbol{\tau}$, the vector of generalized forces.

The generalized forces that a muscle ultimately applies to the body depend on how chemically activated the muscle is, the architectural properties of the muscle (Zajac, 1988; Millard et al., 2013), how it attaches to, and wraps around, the bony geometry of the skeleton (Delp et al., 2007; Scholz et al., 2014). The active tension that a muscle is able to generate varies with its length (Gordon et al., 1966), and lengthening rate (Hill, 1938) and is often described using parametric curves: the active-force-length and force-velocity curves. Though these curves vary from one muscle to another, much of this variation is explained by the differences in the architectural properties of the muscles: the cross sectional area, the optimal fiber length ℓ_o^M, the pennation angle of the fiber, and the tendon slack length. The architectural properties of muscle varies widely from muscle-to-muscle (Arnold et al., 2010). When muscle develops tension it pulls on the bones that it is attached to, and exerts forces across the joints it spans. Muscles that span multiple joints can apply complex, and counter-intuitive generalized forces to the body (Scholz et al., 2014). However, many muscles and groups of muscles are mono-articular and span a single joint in the body. For these mono-articular muscles the active-force-length and force-velocity characteristics can be mapped directly to torque-angle, and torque-angular-velocity characteristics at the joint and used directly to compute the torque applied to a specific joint.

Similar to the work of Forrester et al. (2011) we model the musculature of the sagittal plane model as groups of agonist and antagonist muscle-torque-generators (MTGs). We extend the work of Forrester et al. (2011) by including a parallel elastic element for each MTG, and by modifying the characteristic curves of the MTGs with additional parameters $\mathbf{p}$ (here $\mathbf{p}$ is composed of $\lambda^A, \lambda^P, \lambda^V, s^A, \Delta^P, s^V$, and s^τ terms), explained in the following text, to fit the active and passive properties of the MTGs to data. The normalized active torque developed by a single MTG is given by the product of muscle activation a, the active-torque-angle multiplier t^A, and the torque-velocity multiplier t^V

$$\tau^M(a, \theta, \omega, \mathbf{p}) = s^\tau \tau_o^M \Big(a \mathbf{t}^A(\theta, s^A, \lambda^A) \mathbf{t}^V(\omega, s^V, \lambda^V) \\ + \mathbf{t}^{PE}(\theta, \Delta^P, \lambda^P)(1 - \beta^{PE} \frac{\omega}{s^V \omega_{max}^M}) \Big). \qquad (3)$$

The normalized torque developed by the parallel elastic element is the product of the passive-torque-angle multiplier t^{PE} and a nonlinear damping term which we have added to suppress vibration. Here we use boldface when referring to the characteristic curves of an MTG ($\mathbf{t}^A, \mathbf{t}^V$, and $\mathbf{t}^{PE}$) and normal font when referring to a specific scalar value of a curve (e.g. t^A, t^V, and t^{PE}). The total torque developed by the MTG is the sum of the normalized active element and the normalized parallel elastic element scaled by the maximum isometric torque τ_o^M of the muscle. The fitting parameters λ^A, λ^V, and λ^P are used to blend the curves between a nominal shape and a flat line (Fig. 1A and B); the terms s^A and s^V scale the domain of the $\mathbf{t}^A$ and $\mathbf{t}^V$ curves respectively (Fig. 1C and D); the terms λ^P and Δ^P scale and shift the $\mathbf{t}^{PE}$ curve; and s^τ scales the maximum isometric torque of the subject. These fitting parameters are used to transform the characteristic curves

Curve variation with $\lambda_A, \lambda_P, \lambda_V$
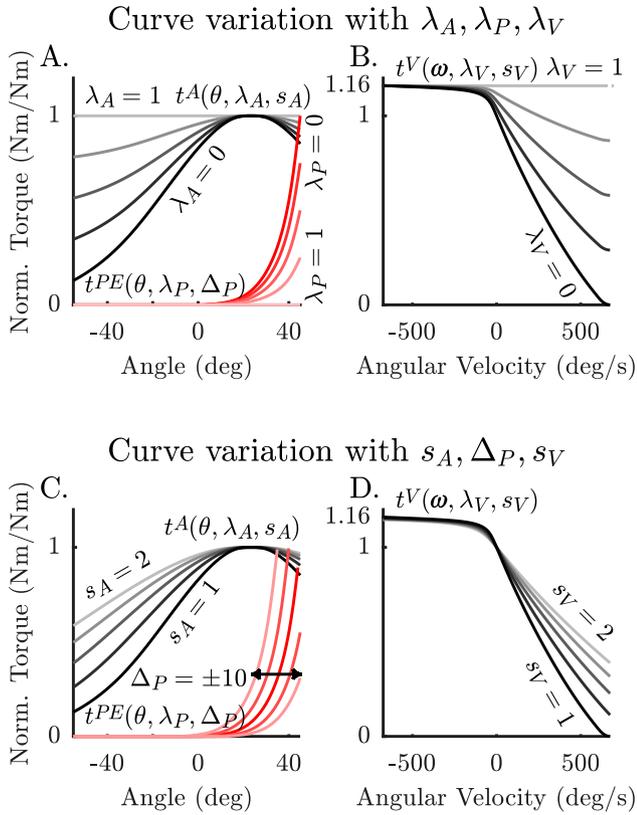
Fig. 1. The torque developed by an MTG depends on the value of the active-torque-angle (t^A) curve, torque-velocity (t^V) curve, passive-torque-angle (t^{PE}) curve, and activation. Each of these curves can be gradually flattened using a blending variable (see λ^A, λ^P, and λ^V in panels A and B). In addition, the domain of the t^A and t^V curves can be stretched using the s^A and s^V parameters; while the t^{PE} curve can be shifted using Δ^P (see panels C and D).

$$\mathbf{t}^A(\theta, s^A, \lambda^A) = \lambda^A + (1 - \lambda^A)\mathbf{t}^A((\theta - \theta_o)/s^A + \theta_o) \tag{4}$$

$$\mathbf{t}^V(\omega, s^V, \lambda^V) = \lambda^V + (1 - \lambda^V)\mathbf{t}^V(\omega/s^V) \tag{5}$$

$$\mathbf{t}^{PE}(\theta, \Delta^P, \lambda^P) = (1 - \lambda^P)\mathbf{t}^{PE}(\theta - \Delta^P) \tag{6}$$

without affecting the underlying equations used to describe the curves.

Most of the parameters in **p** have a physical meaning: increasing s^τ is equivalent to increasing the cross-sectional area of the muscle or increasing the moment-arm of the joint is crosses; increasing s^A and s^V is equivalent to increasing the optimal fiber length of the muscle, or equivalently, reducing the moment-arm of the joint the muscle crosses; changing λ^P and Δ^P is equivalent to altering the flexibility of the muscle. The additional parameters λ^A and λ^V have been introduced to ensure that Eq. (3) can always be solved for an activation a given any τ^M, θ, and ω. In addition, the underlying geometry (5th-order Bézier curves) that defines these curves is continuous to the second derivative making this muscle model compatible with gradient-based optimization methods and thus well suited for motion synthesis. As a note, we have chosen to use affine transformations to transform the curves rather than changing the control points of the Bézier curves directly so that the equations of the curves can be modified (e.g. in case a better fit can be obtained with different curve equations) without affecting the fitting routine.

2.1. Planar whole-body musculoskeletal model

The initial estimates for the parameters of the MTGs for a 16 segment 18 DoF sagittal plane model (Fig. 2) were made primarily
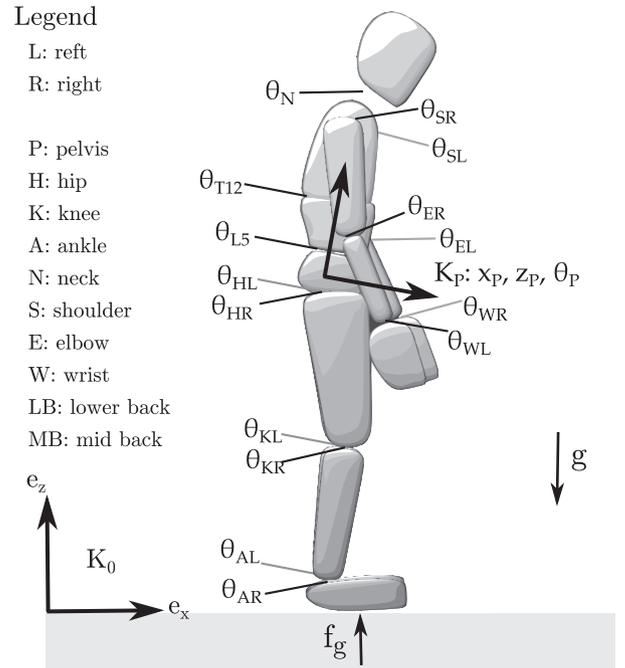
Fig. 2. The human is modelled as a 16 segment 18 DoF planar mechanism. The lumbar spine is treated as a pair of revolute joints at the location of L5/S1 disk and the T12/L1 disk. Planar positions are indicated with x and z, angles with θ.

using dynamometry data collected by Jackson (2010), Anderson et al. (2007) (from the 18–25 year old male data set), and Kentel et al. (2011). The set of parameters for the hip, knee, and shoulder come from the dynamometry data from Jackson (2010) of an elite male gymnast. The parameters for the ankle come from Anderson et al. (2007). To make the strength of the plantar flexors and dorsiflexors consistent with the gymnast that Jackson studied, the maximum isometric torque of the ankle musculature is scaled by the ratio of the knee strength reported by Jackson (2010) to the knee strength reported by Anderson et al. (2007). The characteristics of the musculature that actuates the elbow and wrist come primarily from the dynamometry data from Kentel et al. (2011) of an elite tennis player. The ratio of the shoulder strength reported by Jackson (2010) to that reported by Kentel et al. (2011) is used to scale the strength of the elbow and wrist to make it consistent with the gymnast.

Several data sources were required to establish the characteristics of the MTGs that actuate the lumbar joints. The active-torque-angle curve of the lumbar extensors is fitted to data from Raschke and Chaffin (1996), while the passive-torque-angle curves comes from Dolan et al. (1994). We assume that the gymnast is one standard deviation stronger than the average subject in the study by Dolan et al. (1994) to arrive at the maximum isometric torque of the lumbar extensors. The strength ratio of the lumbar extensors to flexors published by Beimborn and Morrissey (1988) is used to estimate the maximum isometric torque of the lumbar flexors. The maximum angular velocity of the lumbar extensors and flexors is arrived at by using architectural data on the respective moment-arms (7.1 cm & 10.9 cm Németh and Ohlsén (1986)), average optimal fiber lengths (8.08 cm & 29.9 cm Christophy et al. (2012)), and by assuming that these fibers are predominantly slow-twitch with a maximum contraction velocity of $7.02\ell_o^M/s$ Ranatunga (1984). Literature defining the active and passive-torque angle curves for the lumbar flexors (abdominal muscles) could not be found. The lumbar extensors and flexors actuate the two revolute joints (Fig. 2) one representing the L5/S1 joint and the other the T12/L1 joint (Fig. 2). Since the curves we have defined for the lumbar extensors

and flexors apply to the lumbar spine as a whole, we scale the angle and angular velocity of the lumbar joints by two when evaluating evaluating the torque developed by the lumbar extensors and flexors.

2.2. Quadratic program problem formulation

The fitting algorithm adjusts the parameters of the MTGs so that they can produce the same joint torques as the subject with activations that range between 0 and a_{max} (where $a_{max} \leqslant 1$) such that the normalized passive-torque-angle multiplier is less than t_{max}^{PE}. Prior to fitting the MTGs we assume that the multibody model matches the anthropometry of the subject and the recorded motion and forces have been transformed into a time series of generalized positions $\mathbf{q}(t)$, velocities $\dot{\mathbf{q}}(t)$, and forces $\boldsymbol{\tau}(t)$ using inverse dynamics. Further we assume that the strength of the entire set of the MTGs has been scaled roughly to fit the subject given their age, size, and gender. The quadratic problem (QP) described below will only make adjustments to make the MTGs stronger, or more flexible, so that the observed motion can be executed by the model. We have elected to formulate the QP so that it only makes the MTGs stronger or more flexible so that this routine can be used on recordings of sub-maximal efforts without unduly adjusting MTGs that are not, due to the movement, very active or stretched. As a consequence, if the subject is at their strength or flexibility limits during the trial, the reference MTGs should adjusted so that they are both weaker and stiffer than the subject prior to using the fitting method.

To fit the parameters of the ith MTG we first extract τ_{exp}^M, the part of $\boldsymbol{\tau}$ which has the same sign as the direction, u_i^M, as the MTG

$$\tau_{exp}^M(t) = \begin{cases} \tau_{i(t)} & \text{if } \tau_i(t)u_i^M > 0 \\ 0 & \text{otherwise} \end{cases} \tag{7}$$

where u_i^M is either -1 or 1. Here we treat a subset of the parameters $\mathbf{p}$ as optimization variables

$$\mathbf{x} = (s^A, s^V, \Delta^P, \lambda^P, s^\tau). \tag{8}$$

We have excluded λ^A and λ^V from the fitting process because if these parameters are set to large values the active-torque-angle and torque-velocity curves are effectively flattened: this is unrealistic and undesirable. Using the weighting matrix $\underline{W}$ we search for parameters that are as close as possible to the default values $\mathbf{x}_\circ$

$$\min_{\mathbf{x}} (\mathbf{x} - \mathbf{x}_\circ)^T \underline{W}(\mathbf{x} - \mathbf{x}_\circ) \tag{9}$$

and satisfy 3 constraints at each of the *j* time points recorded in the experiment: that $\tau_{exp}^M(t)$ can be generated with an activation no greater than a_{max}

$$(\tau_i^M(a_{max}, \theta(t_j), \omega(t_j), \mathbf{x}) - \tau_{exp}^M(t_j))u_i^M \geqslant 0, \tag{10}$$

that the minimum activation of the muscle is greater than or equal to 0

$$(\tau_{exp}^M(t_j) - \tau_i^M(0, \theta(t_j), \omega(t_j), \mathbf{x}))u_i^M \geqslant 0, \tag{11}$$

and that the passive element does not develop more than t_{max}^{PE}

$$(t_{max}^{PE} - \mathbf{t}^{PE}\theta(t_j), \Delta^P, \lambda^P)u_i^M \geqslant 0. \tag{12}$$

The initial optimization vector is set to $\mathbf{x}_\circ = (1, 1, 0, 0, 1)$ so that the underlying curves match their default values. When this quadratic program (QP) is solved the parameters of the MTG will have been systematically, and minimally adjusted so that the MTG can reproduce the observed loading pattern. Note that as stated, Eq. (7) assumes that agonist-antagonist pairs of MTGs develop no co-contraction. While the parameters λ^A and λ^V are not modified, these

parameters have been set to $\sqrt[4]{\epsilon}$ (where $\epsilon = 2.22 \times 10^{-16}$) so that the Eq. (3) can be solved for activation (given τ^M, θ, and ω) without risk of a numerical singularity. If some level of co-contraction is known, perhaps from EMG recordings of muscle activity, it can be included in the fitting process by modifying Eq. (7).

2.3. Evaluation procedure

To evaluate the fitting routine we used it to fit the MTG parameters described in Section 2 to data of a 35-year old male (mass 81.7 kg, height 1.72 m) stooping (Fig. 3) to pick up a 15 kg box off the floor. We used previously recorded kinematic and force plate data (Millard et al., 2017) and processed it to yield a time series of generalized positions, velocities, and forces. The model fits the subject well as the residual forces and moments of the inverse dynamics analysis are low: 5.4 ± 3.4 N and 3.6 ± 2.5 Nm, with short-lived peaks of 19.3 N and 11.6 Nm when the box is being picked up.

We first assess the default MTG parameters for feasibility by using Eq. (3) and the inverse dynamics data to arrive at an activation time series for each MTG. The value for τ^M in Eq. (3) is not directly taken from the inverse dynamics data, but is first broken up into flexion and extension components using Eq. (7). We set λ^A and λ^V to $\sqrt[4]{\epsilon}$ so that Eq. (3) can be solved for a given values for τ^M, θ, and ω without numerical singularity. The remaining fitting variables are left at the default values of $\mathbf{x}_\circ$. The resulting values of a have a direct physical interpretation: $a < 0$ means that the parallel elastic element of the MTG is too stiff, $a > 1$ means that the active component of the MTG is too weak, and $0 \leqslant a \leqslant 1$ means that the parameters of the MTG are feasible.

We next use the fitting routine described in Section 2.2 to adjust the MTGs so that they can produce the same torques as the subject's musculature during the box lift. We use Eq. (7) to evaluate the torque $\tau_{exp}^M(t)$ and assume that there is no co-contraction between pairs of agonist-antagonist MTGs. While choosing plausible values for a_{max} and t_{max}^{PE} is relatively simple, estimating these parameters accurately for a given subject and task is challenging.

The values for a_{max} for each muscle in a given task can be accurately set if the experimental recordings include EMG data from the task and from a series of MVCs for each muscle of interest. When EMG recordings from the task and an MVC are available, the value of a_{max} for a given muscle is simply the peak value of the filtered rectified EMG signal normalized with respect to the
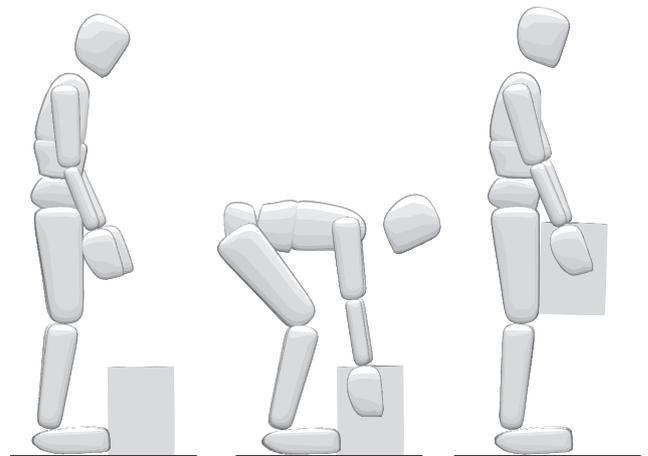
Fig. 3. Inverse kinematics is used to make the model track the positions of the human subject. The subject performed a stoop-lift to pick up the box. At the deepest part of the lift the subject bent his knees but maintained a straight back.

peak value observed during the MVC (Winter, 2009). Unfortunately we do not have EMG recordings from the subject for the task, nor from MVC trials. For the purposes of evaluating the fitting method we set a_{max} to one: any MTG that was previously too weak will, after fitting, be just strong enough to complete the task.

While the value assigned to a_{max} will always affect the fitting result, the value assigned to t_{max}^{PE} may not. The constraint of Eq. (11) that the minimum activation is zero or greater may instead be the limiting factor: when the passive forces of the muscles exceed the $\tau_{exp}^{M}(t)$, the constraint in Eq. (11) will not be satisfied, and as a consequence the solver will adjust the properties of the passive curve. Only motions in which large observed torques $\tau_{exp}^{M}(t)$ happened to be accompanied by large passive torques will be affected by the constraint of Eq. (12).

Here we will set t_{max}^{PE} not to restrict the values of passive forces to subject-specific values, but instead to restrict the upper-bound on passive forces to a reasonable value. Although we are unaware of data which describes the typical tolerance for passive forces, we estimate this upper-bound as being similar to the amount of force tolerated during in-vivo maximally active eccentric contractions: subjects often limit the amount of normalized force (scaled by one divided by maximum active isometric force) to around 1.4 (Yeadon et al., 2006), presumably to avoid injury. In-vitro experiments studying active eccentric contractions (Herzog and Leonard, 2002) show that muscle can tolerate higher forces without causing injury. Thus it is possible that a specific subject might be able to tolerate normalized passive forces greater than 1.4, and that tolerance to high passive forces may vary from subject-to-subject.

To assess the fitted MTGs we first check that the required τ_{exp}^{M} can be generated with activations between 0 and a_{max} and a passive-torque-angle multiplier of less than t_{max}^{PE}. To assess the quality of the fit using a two dimensional figure we project the torque profile onto the θ-τ^{M} plane to see if the torque demand of the task falls within the isometric envelope defined by the active-torque-angle and passive-torque-angle curves. Next, we project the demanded active torque

$$\tau_{A}^{M} = \tau_{exp}^{M} - \mathbf{t}^{PE}(\theta, \Delta^{P}, \lambda^{P})\left(1 - \beta^{PE}\frac{\omega}{s^{V}\omega_{max}^{M}}\right) \qquad (13)$$

onto the ω-τ_{A}^{M} plane to see if the active torque demanded by the task is limited by the torque-velocity curve of the MTG. It is necessary to define τ_{A}^{M} to assess whether τ_{exp}^{M} can be met because only active torque is affected by the limitations of the torque-velocity curve.

We use IPOPT (Wächter and Biegler, 2006) to solve the QP described in Section 2.2 for each of the 30 MTGs using the inverse dynamics data from the box-lift. The QP for each MTG has 5 variables and 588 constraints because there are 196 sample points in the recorded motion. We have set all elements of the diagonal of the weighting matrix $\underline{W}$ to be 1.

3. Results

Prior to fitting the parallel element of the hip extensors is too stiff to allow the model to reach the box with its hands (Fig. 4A): hip flexion angles greater than 81.4° yield negative activations for the hip extensors. The active torque-angle and torque-velocity characteristics of the hip extensor MTG are also too weak to meet the torque demands of the lift in the moments after the box is lifted-off the ground (Fig. 5A and B).

After fitting, the hip extensors are flexible enough to allow the model to grip the box (Fig. 4B) and have sufficient strength to lift the 15 kg box (Fig. 5C & D) with activations between $0 - a_{max}$
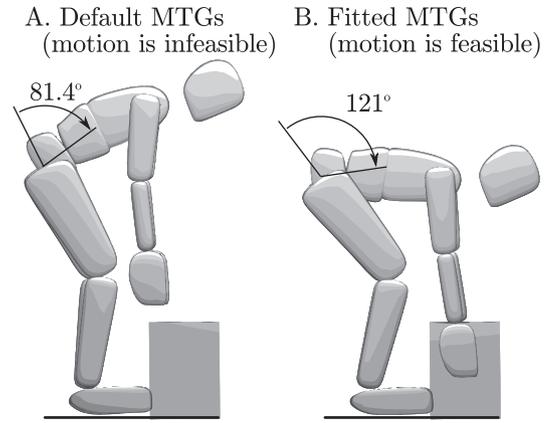
Fig. 4. The parallel element of the default hip extensors are stiff enough that the model cannot reach a hip flexion greater than 81.4° without breaking the constraint of Eq. (11) (panel A). After fitting the model is able to complete the entire motion (panel B), which includes a maximum hip flexion angle of 121°, while satisfying the constraints described in Eqs. (10)–(12).
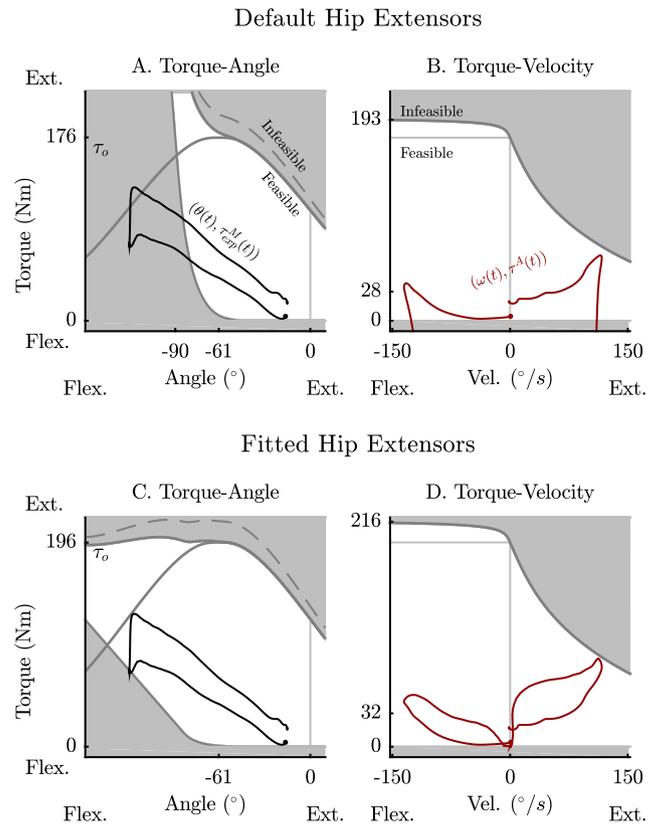
Fig. 5. Prior to fitting the hip extensors are too inflexible and weak to lift the box off the ground (panels A & B). After fitting the feasible region of the muscle has been expanded so that it is strong and flexible enough to complete the observed motion. The region between the dashed and solid grey lines in panels A and C are feasible but only during an active eccentric contraction. Only the right hip extensor MTG is shown, since the left is nearly identical.

(0 − 1). The QP solver made modest adjustments to all of the fitting parameters except for λ^{P} which has been changed substantially (see Table 1). Due to the symmetry of the recorded motion the parameters for the right and left hip extensors agree to 3 significant figures.

The hip extensors require an activation of 1 during the lift when active-torque developed by the MTG hits the boundary of torque-

Table 1
Default and fitted parameters of the right hip extensor.

x	s^A	s^V	Δ^P	λ^P	s^τ
Default	1	1	0	0	1
Fitted	1.03	1.12	$-4.18°$	0.92	1.12

velocity curve (Fig. 5D). The passive-torque-angle multiplier does not approach t^{PE}_{max}. The other MTGs of the musculoskeletal model are feasible for the task and remained unchanged. The entire fitting process required a few seconds of processing on a conventional laptop using an Intel[(R)] central processing unit (i7-3630QM) operating at 2.40 GHz.

4. Discussion

Musculoskeletal models are being used to predict the motion and muscle forces of human subjects for the purposes of research and device design. We have extended the work of Forrester et al. (2011) by adding a parallel-elastic element to the MTG, and by making the underlying equations compatible with gradient-based optimization methods. We have extended the work of King et al. (2009) by developing a method to fit both the active and passive properties of the MTGs to a specific subject. To demonstrate the utility of the MTGs and fitting method we have created a planar whole-body musculoskeletal model using dynamometry data from the literature and have fitted it so that a measured motion can be executed by the model.

The parameters of the MTGs are based on in-vivo dynamometry measurements from several young men (Jackson, 2010; Kentel et al., 2011; Anderson et al., 2007; Dolan et al., 1994; Raschke and Chaffin, 1996). While we are grateful for this data, it is far from complete. Remarkably few studies make measurements across multiple joints of a single subject, measure flexibility, publish raw measurement data, or consider subjects other than young men. We hope and encourage other research groups with these unique facilities and experimental skills to measure multiple joints within a single subject, and to collect data from a broader range of subjects.

The simplifications of the MTG muscle model formulation have necessarily come at a cost: individual fiber kinematics are not represented; bone-on-bone contact forces cannot be calculated; tendon strains are not simulated; the coupling between joints that biarticular muscles introduce is not represented. Despite these simplifications this model is useful for the simulation of many everyday activities, particularly to support the design of wearable robotic systems (Millard et al., 2017) and the tuning of orthoses (Sreenivasa et al., 2017). In the future we plan on extending the musculoskeletal model and fitting method to include line-type muscles that span multiple joints and muscles with elastic tendons.

Conflict of interest

The Authors declare that there are no conflicts of interest related to this work.

Acknowledgments

Appendix A. Gymnast MTG characteristics

This appendix contains the parameters (Table A.2) and plots (Fig. A.6) that define the 14 MTGs that are described in Section 2.1. All of the curves in this dataset are implemented as 5th-order Bézier splines which are continuous to the 2nd derivative throughout their entire domain and closely follow an underlying function. The active-torque-angle splines follow a Gaussian function centered on θ^A_0 and with a standard deviation of θ^A_w, as in Jackson (2010). The passive-torque-angle splines pass through $(\theta^{PE}_0, 0)$ and (θ^{PE}_1, τ_o) and have been shaped to follow the exponential curve used by Jackson (2010). To construct the normalized torque-velocity curve, Hill's hyperbola is first constructed such that it passes through $(\frac{1}{2}\omega^C_{max}, t^V(\frac{1}{2}\omega^C_{max}))$, which allows a fast-twitch or a slow-twitch torque-velocity curve to be easily constructed. The Bézier spline is then fitted to the hyperbola between an angular velocity of 0 and $0.9\omega^M_{max}$. Between $0.9\omega^M_{max}$ and ω^M_{max} the curve is smoothly brought to a value and slope of zero. The eccentric side of the curve is formed such that $t^V(\omega^E_{max})$ is reached at a maximum angular velocity in the eccentric direction with a slope of zero. Note that neither the fitting method nor the muscle model have a dependency on the shape of these curves: if it proves more appropriate to use other curves, such as an asymmetric active-torque-angle curve, this change can be made without affecting the fitting method.

The parameters of the various MTG listed in Table A.2 vary widely from joint-to-joint and from agonist-antagonist: the lumbar extensors are by far the strongest and slowest MTG while the MTG that actuates the wrist in radial deviation are the fastest and weakest. These differences are most clearly observed by looking at plots of the torque-angle and torque-angular velocity characteristics for each of these joints (Fig. A.6).

Appendix B. Example application

This appendix contains a detailed example in which the default MTGs, the fitting routine, motion capture data, and force plate data are used to estimate the lower- and upper-bounds of the leg strength of a child who walks with crouch-gait. We have chosen this subject because he (in contrast to subject used in the box-lifting task) is far weaker than the set of MTGs, and as such, the MTGs need to be pre-weaked prior to using the fitting routine. In addition, this subject also serves as a good example because neither MVCs nor EMG data could be recorded from this clinical patient: conventional EMG-based fitting methods (Lloyd and Besier, 2003; Sartori et al., 2012) cannot be applied to develop a model of this subject.

As mentioned in Section 2.2, the fitting routine can only strengthen the MTG or make it more flexible. While this means the routine can be applied to data collected from a submaximal effort, it also means that the maximum isometric torque of each MTG needs to be slightly weaker than the subject prior to fitting if any adjustment is to be made. As an example, we fit the hip, knee, and ankle MTGs of a sagittal-plane gait model to a 7-year old child who walks with crouch-gait using the data and model of Sreenivasa et al. (2017). Please see the supplementary material for this article to obtain a copy of the script and data required to do the fitting described in this example.

The supplementary data from Sreenivasa et al. (2017) contains one walking trial, 3053176.c3d, in which ground forces are individually recorded under each foot. We prepared the data for fitting by performing an inverse-kinematics analysis, smoothed the generalized positions using a dual-pass 2nd-order low-pass Butterworth filter (10 Hz), used the central-difference method to numerically

Table A.2

Parameters of the characteristic curves of the MTGs. Light grey cells indicate parameters which could not be found in the literature and have been estimated. Light blue cells are passive parameters that have been added to prevent a joint from hyper-extending. For brevity we will indicate the source of data in each case using the leading letter of the first author's name: 'A' for Anderson et al. (2007), 'B' for Beimborn and Morrissey (1988), 'D' for Dolan et al. (1994), 'J' for Jackson (2010), 'K' for Kentel et al. (2011) and 'R' for Raschke and Chaffin (1996).

	$\tau_\mathrm{o}^\mathrm{M}$	$\theta_\mathrm{o}^\mathrm{A}$	$\theta_\mathrm{w}^\mathrm{A}$	$\omega_\mathrm{max}^\mathrm{M}$	$\mathrm{t}^\mathrm{V}(\omega_{max}^E)$	$\mathrm{t}^\mathrm{V}(\frac{1}{2}\omega_{max}^C)$	θ_0^PE	θ_1^PE	
	Nm	°	°	°/s	Nm/Nm	Nm/Nm	°	°	Source
Hip Ext.	176	-61	61	517	1.10	0.16	-45	-90	J, A
Hip Flex.	157	-42	70	526	1.12	0.25	5	30	J, A
Knee Ext.	286	-54	29	1101	1.13	0.12	-115	-155	J, A
Knee Flex.	99	-59	64	953	1.12	0.20	0	10	J, A
Ankle P.Flex.	128	-23	38	674	1.16	0.41	-2	-45	A
Ankle D.Flex.	44	11	35	990	1.27	0.11	30	60	A
Lumbar Ext.	688	-89	66	458	1.10	0.15	-18	-78	R, D
Lumbar Flex.	212	0	360	1102	1.10	0.15	0	45	D, B
Shoulder Ext.	127	-123	105	931	1.10	0.25	-162	-204	J, K
Shoulder Flex.	91	-51	74	1093	1.23	0.25	30	60	J, K
Elbow Ext.	101	-19	207	1037	1.37	0.19	-120	-150	K
Elbow Flex.	70	-94	75	1057	1.32	0.19	0	10	K
Ulnar Dev.	31	-25	85	1032	1.35	0.20	0	30	K, J
Radial Dev.	24	65	147	1247	1.31	0.21	-20	-50	K, J

calculate generalized velocities and accelerations, and finally performed an inverse-dynamics analysis to solve for the resulting generalized forces. Our interval of fitting has been trimmed to include only times in which the feet are in contact with the force-plate or are in swing. The residual forces within this interval are relatively low ($f_X = 0.91 \pm 10.9, f_Y = 13.5 \pm 9.59, \tau_Z = -1.56 \pm 5.23$).

Since we have limited experimental data from this subject, we will establish lower- and upper-bounds on the strength of the musculature at the hip, knee and ankle. The lower-bound on the subject's strength is estimated using the inverse dynamics data and the fitting routine assuming that the hip, knee, ankle extensors reach maximum activation during the walking trial. The upper-bound on the subject's strength is estimated using dynamometry data (Eek et al., 2006) collected from typically developing children of a similar age and size. We are using the leg strength from a typically developing child as an upper-bound on the subject's strength because children who walk with crouch-gait are weak compared to their peers (Wiley and Damiano, 1998).

To solve for the lower-bound on the strength of the leg extensors, we pre-weaken these MTGs from the default value (to 80% of the peak moment) so that the fitting routine is forced to adjust these MTGs to fit the data (upper-panel of column τ_o^{M*} in Table B.3). The default values for all remaining parameters of the extensors are left unchanged. After running the fitting routine on the leg extensors, it is clear that the pre-weakening was adequate as $s^\tau > 1$ in all cases (upper-half of column s^τ in Table B.3). The fitting routine also made adjustments to the s^A and s^V parameters and increased the flexibility of the ankle extensors and left hip extensors (upper-half of columns s^A, s^V, and λ^P in Table B.3). The large change of λ^P for the ankle extensors have been made because of the large dorsi-flexion angle that the subject uses during stance (Fig. B.7) and also because the initial passive-torque-angle curve would have required a very large offset angle to achieve the same result.

To estimate the lower-bound on the strength of the hip, knee, and ankle flexors, we assume that a submaximal activa-

tion is achieved during the recorded walking trial. Rather than estimate the level of submaximal activation, we instead estimate τ_o^M of the flexors and use the fitting routine to check that these parameters are feasible for the subject's gait. We estimate the initial τ_o^M of the flexors by scaling the fitted extensor τ_o^M values by the flexor-to-extensor torque ratios at the hip (0.702), knee (0.533) and ankle (0.347) from the data set of Anderson et al. (2007) for healthy young male subjects (lower-half of column τ_o^{M*} in Table B.3). We have elected to use the flexor-to-extensor ratios from Anderson et al. (2007) because these recordings have been made from typical subjects rather than from an athlete (Jackson, 2010). The results returned by the fitting routine show that modest adjustments have been made to the right and left hip flexors, and the right ankle flexor (lower-half of Table B.3).

We estimate the upper-bound of the subject's strength using the hand-held isometric dynamometry data (Eek et al., 2006) for a control subject of the same age, similar weight (1.5 kg heavier), and similar height (5.4 cm taller) to the subject. We estimate τ_o^M by scaling the hip, knee, and ankle extensor torque measurements of Eek et al. (2006) by t^A (evaluated using the corresponding active-torque-angle-curve) since these recordings are isometric and are in a range where there are no passive forces. As before, the strength of the hip knee and ankle flexors are computed by making use of the same flexor-to-extensor ratios that we used for the subject. The control is far stronger than the lower-bound we established using the subject's data with a pronounced difference at the plantarflexors (Table B.4).

Since crouch-gait is known to be caused by weak plantar flexors (Elder et al., 2003), we expect the true value of the subject's τ_o^M at the ankle extensors to be close to the lower-bound. In contrast, we expect the strength of the hip and knee musculature to lie between the lower- and upper-bounds (Wiley and Damiano, 1998). Even though the data available on the subject is sparse, the fitting routine has allowed us to establish a feasible lower-bound on the strength of the subject's legs.
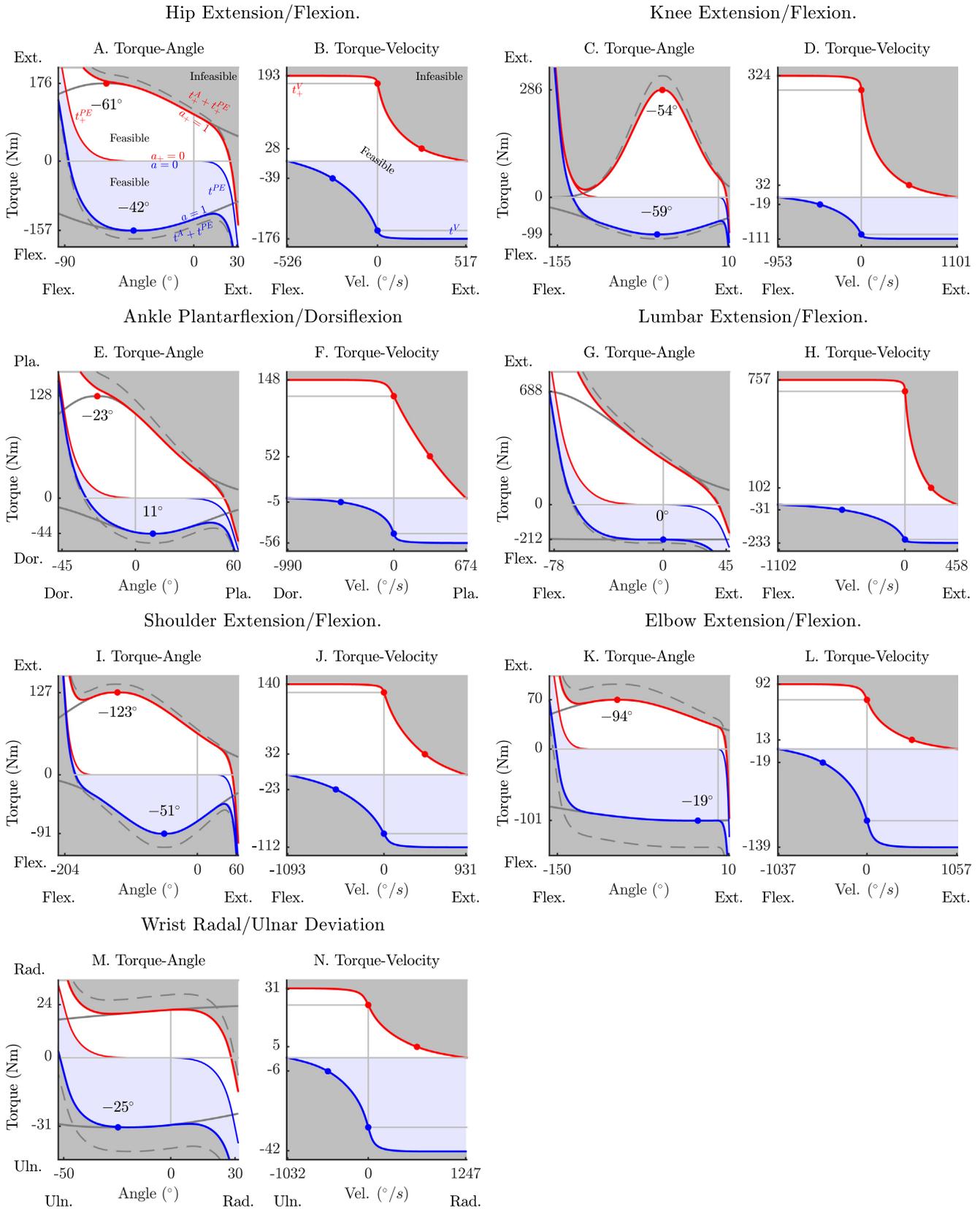
Fig. A.6. The torque-angle and torque-velocity characteristics for agonist and antagonist muscles of the hip, knee, ankle, lumbar, shoulder, elbow and wrist joints. These curves have, with few exceptions, been extracted from data in the literature and modified to ensure continuity to the second derivative. Please see the text of Section 2.1 and the supplementary material for details.

Table B.3
Pre-weakened (τ_o^{M*}) and fitted hip, knee, and ankle MTG parameters. Parameters highlighted in light-grey have been modified by the fitting routine.

	τ_o^{M*} (Nm)	s^A	s^V	Δ^P (°)	λ^P	s^τ
Hip Ext. R.	13.3	1.22	1.51	0.00	0.00	1.81
Knee Ext. R.	14.4	1.00	1.00	0.00	0.00	1.17
Ankle Ext. R.	12.9	1.00	1.00	0.00	1.00	1.17
Hip Ext. L.	19.5	1.22	1.30	0.00	1.00	1.81
Knee Ext. L.	11.7	1.08	1.00	0.00	0.00	1.30
Ankle Ext. L	11.2	1.00	1.05	0.00	1.00	1.31
Hip Flex. R.	16.8	1.04	1.10	0.00	0.00	1.19
Knee Flex. R.	9.00	1.00	1.00	0.00	0.00	1.00
Ankle Flex. R.	5.22	1.08	1.07	0.00	0.00	1.15
Hip Flex. L.	24.8	1.01	1.14	0.00	0.00	1.11
Knee Flex. L.	8.10	1.00	1.00	0.00	0.00	1.00
Ankle Flex. L.	5.08	1.00	1.00	0.00	0.00	1.00

Table B.4
A comparison of the lower-bound (LB) and upper-bound (UB) estimates of the maximum-isometric-torque at the hip, knee, and ankle of the subject. The lower-bound estimate comes from applying the fitting routine to inverse dynamics data from subject while the upper-bound estimate comes from hand-held dynamometry data from a control subject of the same age and a similar size (Eek et al., 2006).

	τ_o^M		
	LB		UB
	Right	Left	
Hip Ext.	13.3	19.5	52.2
Knee Ext.	14.4	11.7	64.6
Ankle Ext.	12.9	11.2	25.5
Hip Flex.	16.8	24.8	36.6
Knee Flex.	9.00	8.10	34.4
Ankle Flex.	5.22	5.08	8.85

improved if additional data is available. Additional data can be used in three ways: to improve the accuracy of the estimate of the maximum activation reached during a trial, to more accurately estimate parameters that are not adjusted by the fitting routine (such as θ_o^A, $t^V(\omega_{max}^E)$), and to improve the initial guess of the parameters of the MTGs parameters prior to fitting. We hope that the fitting method and MTGs that we have developed will help others make more accurate subject-specific models given the data at hand and in the literature.

Appendix C. Supplementary material

Supplementary data associated with this article can be found, in the online version, at https://doi.org/10.1016/j.jbiomech.2019.04.004.

Fig. B.7. Prior to fitting, the weakened left plantarflexor is too weak and stiff to walk as the subject did (panels A & B). After fitting the plantarflexor has been made slightly more flexible and stronger so that the inverse dynamics data is now feasible for the left plantarflexor (panels C & D). Note that the value for τ_A^M is calculated using Eq. (13) described in Section 2.3.

This example illustrates how the fitting routine can be used as a tool to estimate the strength and flexibility of a subject given a sparse amount of data. It should also be clear from the assumptions that we have had to make that the quality of the fitting can be

References

Anderson, D., Madigan, M., Nussbaum, M., 2007. Maximum voluntary joint torque as a function of joint angle and angular velocity: model development and application to the lower limb. J. Biomech. 40 (14), 3105–3113.

Arnold, E., Hamner, S., Seth, A., Millard, M., Delp, S., 2013. How muscle fiber lengths and velocities affect muscle force generation as humans walk and run at different speeds. J. Exp. Biol. 216 (11), 2150–2160.

Arnold, E., Ward, S., Lieber, R., Delp, S., 2010. A model of the lower limb for analysis of human movement. Ann. Biomed. Eng. 38 (2), 269–279.

Beimborn, D., Morrissey, M., 1988. A review of the literature related to trunk muscle performance. Spine 13 (6), 655–660.

Christophy, M., Senan, N., Lotz, J., O'Reilly, O., 2012. A musculoskeletal model for the lumbar spine. Biomech. Model. Mechanobiol. 11 (1-2), 19–34.

Damsgaard, M., Rasmussen, J., Christensen, S., Surma, E., de Zee, M., 2006. Analysis of musculoskeletal systems in the AnyBody modeling system. Simul. Model. Pract. Theory 14 (8), 1100–1111.

De Leva, P., 1996. Adjustments to Zatsiorsky-Seluyanov's segment inertia parameters. J. Biomech. 29 (9), 1223–1230.

De Zee, M., Hansen, L., Wong, C., Rasmussen, J., Simonsen, E., 2007. A generic detailed rigid-body lumbar spine model. J. Biomech. 40 (6), 1219–1227.

Delp, S., Anderson, F., Arnold, A., Loan, P., Habib, A., John, C., Guendelman, E., Thelen, D., 2007. OpenSim: open-source software to create and analyze dynamic simulations of movement. IEEE Trans. Biomed. Eng. 54 (11), 1940–1950.

Dolan, P., Mannion, A., Adams, M., 1994. Passive tissues help the back muscles to generate extensor moments during lifting. J. Biomech. 27 (8), 1077–1085.

Eek, M., Kroksmark, A., Beckung, E., 2006. Isometric muscle torque in children 5 to 15 years of age: normative data. Arch. Phys. Med. Rehabil. 87, 1091–1099.

Elder, G., Kirk, J., Stewart, G., Cook, K., Weir, D., Marshall, A., Leahey, L., 2003. Contributing factors to muscle weakness in children with cerebral palsy. Dev. Med. Child Neurol. 45 (8), 542–550.

Falisse, A., Van Rossum, S., Jonkers, I., De Groote, F., 2017. Emg-driven optimal estimation of subject-specific hill model muscle–tendon parameters of the knee joint actuators. IEEE Trans. Biomed. Eng. 64 (9), 2253–2262.

Forrester, S., Yeadon, M., King, M., Pain, M., 2011. Comparing different approaches for determining joint torque parameters from isovelocity dynamometer measurements. J. Biomech. 44 (5), 955–961.

Gill, P., Murray, W., Saunders, M., 2005. Snopt: an sqp algorithm for large-scale constrained optimization. SIAM Rev. 47 (1), 99–131.

Gordon, A., Huxley, A., Julian, F., 1966. The variation in isometric tension with sarcomere length in vertebrate muscle fibres. J. Physiol. 184 (1), 170–192.

Herzog, W., Leonard, T., 2002. Force enhancement following stretching of skeletal muscle: a new mechanism. J. Exp. Biol. 205 (9), 1275–1283.

Hiley, M., Jackson, M., Yeadon, M., 2015. Optimal technique for maximal forward rotating vaults in men's gymnastics. Hum. Movement Sci. 42, 117–131.

Hill, A., 1938. The heat of shortening and the dynamics constants of muscle. Proceedings of the Royal Society of London, vol. 126, pp. 136–195.

Jackson, M., 2010. The Mechanics of the Table Contact Phase of Gymnastics Vaulting (PhD thesis). Loughborough University.

Jensen, R., 1986. Body segment mass, radius, and radius of gyration proportions of children. J. Biomech. 19 (5), 359–368.

Kentel, B., King, M., Mitchell, S., 2011. Evaluation of a subject-specific, torque-driven computer simulation model of one-handed tennis backhand ground strokes. J. Appl. Biomech. 27, 345–354.

King, M., Kong, P., Yeadon, M., 2009. Determining effective subject-specific strength levels for forward dives using computer simulations of recorded performances. J. Biomech. 42 (16), 2672–2677.

King, M., Wilson, C., Yeadon, M., 2006. Evaluation of a torque-driven model of jumping for height. J. Appl. Biomech. 22 (4), 264–274.

Lloyd, D.G., Besier, T.F., 2003. An emg-driven musculoskeletal model to estimate muscle forces and knee joint moments in vivo. J. Biomech. 36 (6), 765–776.

Millard, M., Sreenivasa, M., Mombaur, K., 2017. Predicting the motions and forces of wearable robotic systems using optimal control. Front. Robot. AI 4, 41.

Millard, M., Uchida, T., Seth, A., Delp, S., 2013. Flexing computational muscle: modeling and simulation of musculotendon dynamics. J. Biomech. Eng. 135 (2), 021005.

Nakamura, Y., Yamane, K., Fujita, Y., Suzuki, I., 2005. Somatosensory computation for man-machine interface from motion-capture data and musculoskeletal human model. IEEE Trans. Robot. 21 (1), 58–66.

Németh, G., Ohlsén, H., 1986. Moment arm lengths of trunk muscles to the lumbosacral joint obtained in vivo with computed tomography. Spine 11 (2), 158–160.

Ranatunga, K., 1984. The force-velocity relation of rat fast-and slow-twitch muscles examined at different temperatures. J. Physiol. 351 (1), 517–529.

Raschke, U., Chaffin, D., 1996. Support for a linear length-tension relation of the torso extensor muscles: an investigation of the length and velocity EMG-force relationships. J. Biomech. 29 (12), 1597–1604.

Sartori, M., Reggiani, M., Farina, D., Lloyd, D., 2012. Emg-driven forward-dynamic estimation of muscle force and joint moment about multiple degrees of freedom in the human lower extremity. PloS One 7 (12), e52618.

Scholz, A., Stavness, I., Sherman, M., Delp, S., Kecskeméthy, A., 2014. Improved muscle wrapping algorithms using explicit path-error Jacobians. In: Computational Kinematics. Springer, pp. 395–403.

Sreenivasa, M., Millard, M., Felis, M., Mombaur, K., Wolf, S.I., 2017. Optimal control based stiffness identification of an ankle-foot orthosis using a predictive walking model. Front. Comput. Neurosci. 11, 23.

Steele, K., Seth, A., Hicks, J., Schwartz, M., Delp, S., 2010. Muscle contributions to support and progression during single-limb stance in crouch gait. J. Biomech. 43 (11), 2099–2105.

Thelen, D.G., 2003. Adjustment of muscle mechanics model parameters to simulate dynamic contractions in older adults. J. Biomech. Eng. 125 (1), 70–77.

van den Bogert, A., Geijtenbeek, T., Even-Zohar, O., Steenbrink, F., Hardin, E., 2013. A real-time system for biomechanical analysis of human movement and muscle function. Med. Biol. Eng. Comput. 51 (10), 1069–1077.

van den Bogert, A., Samorezov, S., Davis, B., Smith, W., 2012. Modeling and optimal control of an energy-storing prosthetic knee. J. Biomech. Eng. 134 (5), 051007.

van der Helm, F., 1997. A three-dimensional model of the shoulder and elbow. In: First Conference of the International Shoulder Group. Shaker Publishing BV, Delft, The Netherlands, pp. 65–70.

Wächter, A., Biegler, L., 2006. On the implementation of an interior-point filter line-search algorithm for large-scale nonlinear programming. Math. Program. 106 (1), 25–57.

Wiley, M.E., Damiano, D.L., 1998. Lower-extremity strength profiles in spastic cerebral palsy. Develop. Med. Child Neurol. 40 (2), 100–107.

Winter, D., 2009. Biomechanics and Motor Control of Human Movement. John Wiley & Sons.

Yeadon, M., King, M., Wilson, C., 2006. Modelling the maximum voluntary joint torque/angular velocity relationship in human movement. J. Biomech. 39 (3), 476–482.

Zajac, F., 1988. Muscle and tendon: properties, models, scaling, and application to biomechanics and motor control. Crit. Rev. Biomed. Eng. 17 (4), 359–411.